SUPPORTING INFORMATION

The Science of Water Leaks: Validated Theory for Moisture Flow in Micro- and Nano-channels

Wenwen Lei [†], *Nicole Fong* [†], *Yongbai Yin* [†], *Martin Svehla* [‡] *and David R. McKenzie* *[†]

[†] School of Physics, University of Sydney, NSW, 2006, Australia

[‡] Cochlear Limited, 1 University Ave., Macquarie University, Sydney, NSW 2109, Australia.

*Corresponding author: david.mckenzie@sydney.edu.au

1. Materials and Methods

1.1 The Two-Chamber Method for Water Vapor Flow Rate Measurements

The two chamber method was used to investigate type *a* and type *b* leaks (shown in Fig. 1 in the main article) in 25 μm microchannels.

1.1.1 Experimental Apparatus

The volume of Chamber 2 was measured using an additional known volume reference, to obtain a result of 447.6234 ml with a standard error of 0.0098 ml. The pressure in Chamber 2 was measured by an appropriately selected MKS Capacitance Manometers with maximum pressure readings of 133 Pa, 1333 Pa, 13333 Pa or 133333 Pa. The accuracy of the capacitance manometer was better than 0.5% of the reading. The pressure in Chamber 2 was recorded as a function of time under isothermal conditions at 295.5 ± 2 K over a period of at least 4 hours using Labview software. The temperature of the surrounding air was logged together with the pressure.

The uncertainties of measurement in the constant volume technique arise principally from the exchange of gases with the walls of Chamber 2 while the test is running. The pressure in Chamber 1 was found to be relatively stable over periods of several hours at the operating pressure. The small outgassing of the walls is effectively balanced by the small outflow through the microchannel. The leak rate of the two-chambers was checked by helium leak detection (QMS 200) and was found to be less than the detection limit (~5.3×10^{-12} kg/s). Since the saturation pressure of water vapor at 295.5 K is 2702.3 Pa, the maximum input pressure was 2128 Pa. Water vapor mass flow rates in the range of 1×10^{-13} to 1×10^{-15} kg/s were possible for measurement.

As the length of the channel is much larger than the diameter, end effects were neglected. The largest Reynolds number in this study was 1.036×10^{-2} ensuring laminar flow.

1.1.2 Test Method

For isothermal conditions, and for pressures less than saturation pressure, the water vapor in the chambers can be described by the ideal gas law:

$$P_2 V_2 = m k_B T \tag{1}$$

where P_2 and V_2 are the pressure and volume of Chamber 2, m is the molecular mass of the test gas, usually water vapor, k_B is the Boltzmann constant, and T is the test temperature. From Eq.(1),

$$\frac{dP_2}{P_2} = \frac{dm}{m} + \frac{dT}{T} \tag{2}$$

We can obtain the mass flow rate by combining Eqs.(1) and (2):

$$\dot{m} = \frac{dm}{dt} = \frac{V_2}{k_B T}\frac{dP_2}{dt}(1-\delta); \quad \delta = \frac{dT/T}{dP_2/P_2} \tag{3}$$

If δ is smaller than 1, an uncertainty estimate is obtained following Ewart et al. [1] For our experiments, the temperature variation is 2 K and pressure variation is 2%, giving a value of δ of the order of 0.34. In order to determine the mass flow rate, the only unknown parameter in Eq. (3) is $\frac{dP_2}{dt}$, obtained from a linear fitting of experimental data as a function of time:

$$P_{2f}(t) = at + b \tag{4}$$

The uncertainty in the coefficient a is $\pm 0.5\%$ for our experiments. Thus, we can obtain a total uncertainty in mass flow rate of $\pm 3.24\%$ ($\frac{\Delta V}{V} = \pm 2.1\%$, $\frac{\Delta T}{T} = \pm 0.67\%$, $\frac{\Delta a}{a} = \pm 0.5\%$).

1.1.3 Adsorption on the Walls of the Apparatus

Water vapor adsorbs strongly on stainless steel walls. Because of adsorption, the pressures in chambers decreased once water vapor entered the test chambers. Deitz and Turner have showed that water vapor obeys a BET adsorption isotherm on stainless steel [2].

Since the pressure in Chamber 2 is much lower than the saturation pressure in our test, the adsorption rate is initially rapid and then trends to a constant value.

In water vapor experiments (P_1 = 119.7 Pa, P_2 = 39.9 Pa shown in Fig. S1), two Stages can be defined. In Stage I the adsorption rate is faster than the flow rate through the channel and in Stage II the adsorption rate is slower than the flow rate. There is also desorption in both stages. We define the sum of adsorption and desorption as a background "outgassing rate". The flow rate is measured by determining the rate of rise of pressure in Chamber 2 and subtracting the outgassing rate. A typical result for the outgassing rate is shown as the black dots in Fig. S1 and a typical result for the flow rate plus the outgassing rate are shown as the red dots also in Fig. S1. The flow rate measurement begins when there is a departure from the background outgassing rate. Since the adsorption rate is dependent on the input pressure, each measurement of input pressure of water vapor needs to be accompanied by a measurement of the corresponding "outgassing rate". The outgassing rate is measured for each run by replacing the channel with a blank vacuum tight plate.

1.2 Mass Loss Method

The vials were used to form leaks of different types are shown in Fig. 1(b) in the main article. A type *a* leak was formed when the vial was held upright, the microchannel did not contact the surface of the liquid in the vial and the glycerol content of the liquid was sufficient to lower the vapor pressure below the saturation pressure to prevent liquid condensing in the channel. A type *a* leak could be operated in a desiccator with air filling the vial and the space outside the vial or alternatively, in the absence of air when the vial was located upright in a vacuum system and the air was removed from both the vial and the space around it. A type *b* leak was formed when the vials were held upright, the microchannel did not contact the liquid surface and the liquid was pure water. The type *b* leak could be operated in either air or vacuum. A type *c* leak was formed when the microchannel inlet was

in contact with the liquid surface of pure water. This leak type was operated in an upright condition. Operation in both air and vacuum was used. In the case of operation in vacuum, it was assumed that the liquid at the inlet remained at 1 atm pressure, because of the air filling the vial. The type *c* leak requires a meniscus at the outlet side of the liquid slug and it could be achieved with 1.7 μm channels operating into both vacuum and air and with 25 μm channels operating in air. In the case of 25 μm channels, a type *c* leak operating into vacuum could not be realized, since the Poiseuille flow rate exceeds the meniscus evaporation rate and the channel fills, operating as a type *d* leak. The type *d* leak was formed by operating the vial in vacuum in an either an inverted or upright condition. This leak type was operated with a 1 atm pressure gradient across the microchannel since the air filling remains after the vial is placed in vacuum. The experimental results for all are shown in Table S1 for 25 μm channels, Table S2 for 10 and 50 μm channels, and Table S3 for 1.7 μm channels.

The uncertainties for the mass loss method are derived from the departures from an average value of the results for the same relative humidity. An example was shown in Figure S2 for an experimental set (vials with one, two and three tubes through lids) in desiccator at room temperature with saturation pressure of water vapor as partial pressure difference and without total pressure difference across the tubes. The flow rate for this case is relatively large and unstable, leading to a large uncertainty shown in Figures 3(a) and (b) in the main article. Note that the experimental results shown in Figure 3(c) have been taken under the same conditions as in Figure S2. The only difference is that there are “surges” occurring for the results in Figure 3 (c) which causes scatter in flow rates.

1.3 Mass Spectrometry Method

The test system was a two chamber configuration, as schematically illustrated in Fig. 1(c) in the main article, primarily constructed using stainless steel CF40 vacuum components. Chamber 1 was used for test gas/vapour input and Chamber 2 was located downstream of

Chamber 1, attached to an RGA (MKS Microvision 2) for gas analysis. The test sample was located between the two chambers. A turbomolecular pump (Pfeiffer HiPace 80 with TC110) was used under constant operation to maintain a background vacuum pressure in Chamber 2 $< 5 \times 10^{-7}$ mbar. Similarly, a diaphragm pump (Pfeiffer MVP015-2) was used to evacuate Chamber 1 to background pressures < 4 mbar. Heating tapes were wrapped around both chambers and maintained at 140 ± 5 ℃ to maintain low background water levels. For D_2O and helium experiments, D_2O (Sigma Aldrich, USA) or helium was injected into Chamber 1. For helium tests, the gas was injected into the chamber with constant flow to maintain a 1 bar pressure. D_2O was injected via a valve into the chamber, which at 140 ℃ exceeds the vapour pressure of D_2O. RGA data was collected for each test run for 1 to 33 AMU using Process Eye Professional software over a period of 72.8 hours with a sensitivity of 4.5×10^{-2} A/mbar. Background spectra as well as spectra for a 10^{-7} mbar.L/s helium calibrated leak (Adixen, France) were obtained prior to D_2O and helium experiments to ensure the system was free from air leaks and/or contaminants and that the RGA was operating consistently.

1.4 Leaks in Pt feedthroughs in alumina blocks

The Pt wires formed hermetic seals when tested initially with He. Some of the seals we found to be leaking using helium testing. In some of the others, leaks were induced by soaking the alumina blocks in 70% w/w ethanol/water for two weeks, which induced leaks in many of the blocks. Helium leak testing was used to detect the leaks. In some of the remainder, leaks could be induced by further soaking. The process for sealing the Pt wires in the alumina blocks has been described in a paper [3].

2. Basic Theory

2.1 Surface Flows

Surface flows take place when there is a laterally imposed concentration gradient on an adsorbed layer. The mass flow conductance arising from diffusion in a surface layer is based on the result of Gilliand et al. [4]:

$$C_{surface} = \frac{2\pi r_c D_s m}{L} \frac{d\Gamma}{dP} \tag{5}$$

where D_s is the surface diffusion coefficient. For P/P_s of less than 0.1 the slope $\frac{d\Gamma}{dP}$ of the isotherm for water on silica is small. The value of D_s is likely to be small for the initial adsorbed layers. A value of D_s for water vapor on mica has been reported of 3.85×10^{-16} m^2s^{-1} at a P/P_s of 0.14 using atomic force microscopy [5]. In order to obtain an upper limit for the contribution of surface flows at low P/P_s, the highest value from the range of reported values [4] gives a surface mass conductance of the order of 5×10^{-24} m s. This very small value can be safely ignored in comparison to the vapor phase flow for small P/P_s. However, when P/P_s exceeds approximately 0.6, $\frac{d\Gamma}{dP}$, increases sharply, as D_s and surface flows are expected to play a role. The linear dependence of the surface flow conductance in Eq.(5) on the channel radius r_c causes the surface flow to dominate for very small channel diameters, since all other flow conductances have a higher order dependence than linear on channel radius.

2.2 Classical and Modified Poiseuille Law

Liquid water flow in a channel consisting of a capillary of constant sectional area is in most cases well described by the classical Poiseuille law (Eq.(6a)) that assumes no-slip boundary conditions. Recently, the classical Poiseuille law has been challenged by measurements in carbon nanotubes and aquaporin channels [6] [7] [8]which have ultra-smooth walls, causing a slip boundary condition that enhances the flow rate. In this case, the classical Poiseuille law has to be modified with an extra term as shown in Eq. (6b). The classical and

modified Poiseuille laws for liquid flow are expressed as a mass conductance defined by $\dot{m}/\Delta P$:

$$C_L = \frac{\pi {r_c}^4 \rho}{8\eta L} \quad (6a)$$

$$C_L = \frac{\pi {r_c}^4 \rho}{8\eta L}\left(1 + \frac{4\varsigma}{r_c}\right) \quad (6b)$$

where r_c is the radius of the flow channel, ρ is the density of water, η is the dynamic viscosity, L is the channel length and ς is the slip length. The parameter ς characterizes the hydrodynamic boundary condition of the liquid at the channel wall. An expression for the slip length in terms of microscopic parameters describing the nature of the wall has been derived from considerations of the friction at the interface by Bocquet and Barrat [9]. The effect of slip flow becomes more significant for small channels because of the dependence on ${r_c}^3$ of the term in Eq.(6b) that contains the slip length, which dominates the term in ${r_c}^4$.

2.3 Evaporation Rate of a Meniscus

We use the information given by Fig. 2 of Birdi and Vu [10] to calculate the evaporation rate of a meniscus in air. The evaporation rate is determined by the diffusion rate of the water vapor away from the surface. Eq. (2) of the main article is restated here:

$$\dot{m} = 4\pi r_c m D \Delta c \quad (7)$$

The evaporation rate is calculated from a specific case taken from Birdi and Vu, where r_c = 2.0633 $\times 10^{-3}$ mm, $\dot{m}$ = 1.9573 $\times 10^{-9}$ kg at a test temperature 295 K with saturation pressure of 2612 Pa. The diffusion coefficient is evaluated as D = 3.9238 $\times 10^{-6}$ m^2 s. Using this value in our case, the mass conductance of a meniscus operating in air is derived. For a meniscus evaporating into vacuum, Eq. (7) (Eq.(2) in the main article) also applies. The diffusion coefficient in vacuum is obtained from Fick's law [11] which is 1.5240 $\times 10^{-4}$ m^2 s.

2.4 Analysis of Results in the Literature for Flow Rates of Nanodimensioned Channels

While there are no results in the literature for the flow of moisture through individual channels of nanometer dimensions, there are results for media containing carbon nanotubes and for other porous membranes and media containing arrays channels of known diameter. However, care is required in converting the results obtained in these cases to a molar flow rate through an individual channel. Majumder et al. [7, 12] quote results for volume permeance of a carbon nanotube membrane in units of $cm^3cm^{-2}min^{-1}bar^{-1}$ (dimensionally MT^{-3}). We converted their results for volume permeance to molar flow rate (see next section for unit conversions) through an individual channel using data supplied in their supplementary information together with their estimated pore density (details see Table S4) and the quoted membrane thickness which we used as the channel length. Note that in their main paper the results for permeance are incorrectly described as "permeability". This error is also found in Holt et al. [6]. Volume permeability is defined in the ASTM standard with SI units of $m^3\ m^{-1}\ s^{-1}\ Pa^{-1}$ (dimensionally MLT^{-3}). The papers from Majumder et al. and Holt et al. both give an enhancement factor between the experimental and theoretical results. Majumder et al. used the enhancement factor for flow velocity and Holt et al. used the enhancement factor for volume flow rate. We calculated the enhancement factor for volume flow rate based on the information given by Majumder et al. which is ~49814. After converting the enhancement factors to the molar flow rate, the results of Majumdar et al. are well aligned with the results of Holt et al. for carbon nanotubes and with the theoretical results of Li et al. [13], Thomas and McGaughey [14] and Thomas et al. [15] when plotted in our Fig. 1 as a function of channel diameter in the main article.

3. Unit Conversions

The units we used in the main article for flow rate (mole/s) is easily converted to other units used in the literature, as shown below. The conversion factor here is only applicable to water. For molar flow rate of a single channel, the result obtained here should be divided by pore.

From (cm^3/cm^2 bar min) to (mol/s):

(1) From (cm^3/cm^2 bar min) to (mol/m^2 Pa s):

1 (cm^3/cm^2 bar min) = 9.2593×10^{-5} (mol/ m^2 Pa s)

(2) From (mol/ m^2 Pa s) to (mol/s):

1 (mol/ m^2 Pa s) × sample area × pressure difference

From (mbar L/s) to (mol/s):

1 (mbar L/s) =4.41×10^{-4} (mol/s)

Using the first conversion factor, we obtain molar flow rates of the carbon nanotubes from Fig. S7 of Majumder et al. [12], Figure 5 of Du et al. [16] and Figure 4 of Holt et al. [6] shown in Table S4.

References and Notes

1. Ewart, Timothée; Perrier, Pierre; Graur, Irina; Gilbert Méolans, J., Mass flow rate measurements in gas micro flows. *Exp. Fluids.* **2006,** *41*, 487-498.
2. Deitz, Victor R.; Turner, Noel H., Introduction of water vapor into vacuum systems and the adsorption by the walls. *J. Vac. Sci. Technol.* **1970,** *7* (6), 577-580.
3. Lu, H.; Svehla, M. J.; Skalsky, M.; Kong, C.; Sorrell, C. C., Pt-Al2O3 interfacial bonding in implantable hermetic feedthroughs: morphology and orientation. *Journal of biomedical materials research. Part B, Applied biomaterials* **2012,** *100* (3), 817-24.
4. Gilliland, Edwin R.; Baddour, Raymond F.; Perkinson, George P.; Sladek, Karl J., Diffusion on surface. I. Effect of concentration on the diffusivity of physically adsorbed gases. *Ind. Eng. Chem. Fundam.* **1974,** *13*, 95-100.
5. Xu, Lei; Lio, Anna; Hu, Jun; Ogletree, D. Frank; Salmeron, Miquel, Wetting and capillary phenomena of water on mica. *J. Phys. Chem. B* **1998,** *102*, 540-548.
6. Holt, J. K.; Park, H. G.; Wang, Y.; Stadermann, M.; Artyukhin, A. B.; Grigoropoulos, C. P.; Noy, A.; Bakajin, O., Fast mass transport through sub-2-nanometer carbon nanotubes. *Science* **2006,** *312*, 1034-1037.
7. Majumder, Mainak; Chopra, Nitin; J.Hinds, Bruce, Mass transport through carbon nanotube membranes in three different regimes: Ionic diffusion and gas and liquid flow. *ACS Nano* **2011,** *5*, 3867-3877.
8. Murata, K.; Mitsueka, K.; Hiral, T.; Walz, T.; Agre, P.; Heymann, B.; Engel, A.; Fujiyoshi, Y., Structural determinants of water permeation through aquaporin-1. *Nature* **2000,** *407*, 599-605.
9. Bocquet, Lyd ric; Barrat, Jean-Louis, Flow Boundary Conditions from Nano- to Micro-Scales. *Soft Matter* **2007,** *3*, 685-693.
10. Birdi, K. S.; Vu, D. T., A study of the evaporation rates of small water drops placed on a solid surface. *J. Phys. Chem.* **1989,** *93*, 3702-3703.
11. Chapman, Sydney; Cowling, T . G., *The Mathematical Theory of Non-Uniform Gases*. 3 ed.; Cambridge University Press: UK, 1970.
12. Majumder, Mainak; Chopra, Nitin; Andrews, R.; Hinds, B. J., Enhanced flow in carbon nanotubes. *Nature* **2005,** *438*, 44.
13. Li, Yuxiu; Xu, Jinliang; Li, Dongqing, Molecular Dynamics Simulation of Nanoscale Liquid Flows. *Microfluidics Nanofluidics* **2010,** *9*, 1011-1031.
14. Thomas, John; McGaughey, Alan, Water Flow in Carbon Nanotubes: Transition to Subcontinuum Transport. *Phys. Rev. Lett.* **2009,** *102* (18).
15. Thomas, John A.; McGaughey, Alan J. H.; Kuter-Arnebeck, Ottoleo, Pressure-driven water flow through carbon nanotubes: Insights from molecular dynamics simulation. *Int. J. Term. Sci.* **2010,** *49*, 281-289.
16. Du, F.; Qu, L.; Xia, Z.; Feng, L.; Dai, L., Membranes of vertically aligned superlong carbon nanotubes. *Langmuir* **2011,** *27*, 8437-43.

Table S1 Experimental results of water vapor conductance shown in Fig. 2 in the main article for channels with 25 μm diameter and 1 cm length under the condition that microchannels were above liquid water surface. The mass conductance for microchannels under liquid water surface is 9.88271e-13 m s.

25 μm				**25 μm (exposed)**			
P_m/P_s	P_i(Pa)	P_o(Pa)	C(m s)	P_m/P_s	P_i(Pa)	P_o(Pa)	C(m s)
0.4675	1895.2510	631.7504	4.4500e-15	0.0428	173.5044	57.8348	1.1976e-15
0.3922	1589.9970	529.999	1.6110e-15	0.0198	80.2255	26.7418	1.6605e-15
0.2929	1187.1670	395.7223	2.3148e-15	0.0110	44.5112	14.8371	1.2216e-15
0.0967	391.9658	130.6553	2.7823e-15	**25 μm (heated)**			
0.0280	113.5075	37.8358	7.6274e-15	0.0206	82.7872	28.3051	6.9592e-16
0.0092	37.0926	12.3642	1.9252e-14	0.0130	52.7052	17.5587	8.3049e-16
0.0071	28.9039	9.6346	9.8088e-15	0.0058	22.9744	8.5413	1.2792e-15
0.0061	24.6879	8.2293	1.7379e-15	0.0038	15.9773	4.3039	2.3748e-15
0.0030	11.9588	3.9863	3.1758e-15	0.0025	11.0816	2.2025	3.8773e-15
Mass loss method operating in vacuum				0.0018	8.2832	1.4564	3.3424e-15
0.5	2702.3	0	4.9414e-14	0.0019	7.9335	2.5749	6.9222e-15
0.0984	532	0	1.2770e-16	8.67e-04	3.7360	0.9483	8.5155e-15
0.0788	425.6	0	1.4082e-16	7.68e-04	3.0364	1.1172	8.4363e-15
Mass loss method operating in air				5.66e-04	2.6866	0.3711	7.7077e-15
0.5	2702.3	0	2.6110e-15 1.0733e-15 2.3615e-15 1.1657e-15				
0.3937	2128	0	1.5515e-17				
0.3199	1729	0	1.7975e-17				
0.1846	997.5	0	1.2570e-17				
0.1427	771.4	0	1.2264e-17				
0.0788	425.6	0	8.4878e-18				

Table S2 Experimental results of water vapor conductance shown in Fig. 2 in the main article for channels with 10 and 50 μm diameter and 1 cm length under the condition that microchannels were above liquid water surface.

10 μm			
P_m/P_s	P_i(Pa)	P_o(Pa)	C(m s)
0.0224	111.3277	9.6944	7.5498e-16
0.0066	29.0884	6.5409	3.6475e-15
0.0057	26.0986	4.7109	5.2226e-15
0.0029	12.4688	3.2199	2.6198e-15
0.0027	13.8107	0.9137	7.1725e-15
50 μm			
24.4787	10.6400	0.0065	1.2829e-15
14.8880	7.1820	0.0041	3.6360e-15
9.3991	3.9900	0.0025	5.8791e-15
50 μm (heated)			
0.0762	321.1551	90.9188	9.1073e-16
0.0511	209.4750	66.7487	1.1265e-15
0.0394	152.9500	59.9830	6.8878e-16
0.0155	54.2108	29.5925	9.7443e-16
0.0103	40.8244	14.7630	1.8368e-15
0.0082	34.0999	10.1014	1.9185e-15
0.0053	20.6509	7.9800	3.1011e-15
0.0034	13.2854	5.1471	5.0680e-15
0.0024	9.3991	3.3250	5.3880e-15
0.0021	8.3883	2.7105	4.6705e-15
9.62e-04	4.1842	1.0161	6.1733e-15

Table S3 Experimental results of water vapor conductance shown in Fig. 1 in the main article for channels with 1.7 μm diameter and 1 mm length.

P_m/P_s	P_i(Pa)	P_o(Pa)	Molar flow rate (mol/s)
Mass loss method operating in vacuum under the condition that channels were above liquid water surface			
0.5	2702.3	0	1.23025e-8
Mass loss method operating in vacuum under the condition that one end of the channels were immerged in liquid water			
NA	10^5+Laplace pressure	0	inverted: 3.89846e-9 upright: 1.01797e-8
Mass loss method operating in air under the condition that channels were above liquid water surface			
0.5	2702.3	0	1.63327e-10
Mass loss method operating in air under the condition that one end of the channels were immerged in liquid water			
NA	Laplace pressure	0	1.30988e-11

Table S4 Molar flow rate of carbon nanotubes from the literature and the converted results for 1 mm length channel under 1 atm as pressure difference.

Brief summary of literature	Molar flow rate (mole/s) of single channel
Majumder et al. [12]: Pore diameter = 7 nm Permeance = 0.58 cm^3/cm^2 ꞏbar ꞏmin Sample area = 0.785 cm^2 Pore density = 1×10^9 $/cm^2$ Pressure difference = 0.8 bar	4.296×10^{-13}
Du et al. [16]: Pore diameter = 10 nm Permeance = 3.83 cm^3/cm^2 ꞏbar ꞏmin Sample area = 0.72 cm^2 Pore density = 2.4×10^{10} $/cm^2$ Pressure difference = 1 bar	1.476×10^{-13}
Holt et al. [6]: Pore diameter = 1.6 nm Permeance = 7.6857 mm^3/cm^2 atm s Sample area = 175,000 μm^2 Pore density = 2.5×10^{11} $/cm^2$ Pressure difference = 0.82 bar	1.399×10^{-15}

Figure S1 An example of the pressure change in Chamber 2 with time during a flow test (red line). The inlet pressure is 119.7 Pa and the outlet pressure is 39.9 Pa. The black line shows the outgassing rate of Chamber 2 in the absence of a flow channel.

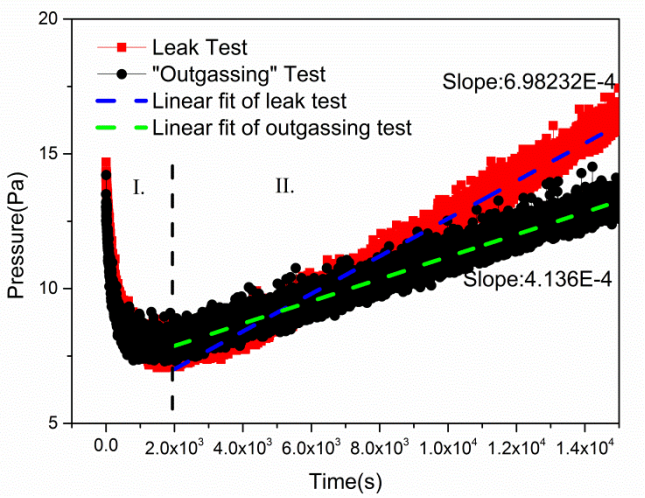

Figure S2 An example for uncertainty analysis for the mass loss method ($P_i = P_s$, $P_o = 0$).